RC25520 (OTH1502-001) February 9, 2015
Electrical Engineering

IBM Research Report

Blind Calibration for Radio Interferometry Using Convex Optimization

S. Kazemi
IBM Research – The Netherlands
Postbus 9999
1006 CE Amsterdam
The Netherlands

P. Hurley, O. Öçal, G. Cherubini
IBM Zurich Research Laboratory
8803 Rüschlikon
Switzerland

Research Division
Almaden – Austin – Beijing – Brazil – Cambridge – Dublin – Haifa – India – Kenya – Melbourne – T.J. Watson – Tokyo – Zurich

BLIND CALIBRATION FOR RADIO INTERFEROMETRY USING CONVEX OPTIMIZATION

S. Kazemi[1], *P. Hurley*[2], *O. Öçal*[2], *G. Cherubini*[2]

[1]IBM Research, The Netherlands, Postbus 9999, 1006 CE Amsterdam, the Netherlands
[2]IBM Zurich Research Laboratory, 8803 Rüschlikon, Switzerland

ABSTRACT

Radio interferometric arrays as imperfect instruments require calibration to correct for instrumental gain and phase errors in observations. One point of calibration, our focus, is before the time-series of groups of compact receivers are beam-formed.

Traditional supervised calibration approaches tune instrumental parameters using prior sky source information. This can prove problematic when information is either insufficiently accurate or missing.

We propose to apply the blind (unsupervised) calibration approach for compressed sensing in the calibration of compact phased-arrays. The approach exploits a sparsity description of the sky, using no prior knowledge of actual objects within. Simulations as well as real-data analysis admit that the blind calibration approach is indeed an improvement over existing supervised calibration methods.

Index Terms— Calibration, radio interferometry, phased-array, sparsity, station

1. INTRODUCTION

Radio interferometry is the technique that combines measurements of multiple antennas so as to achieve upgraded resolution in astronomical observations [1, 2]. The new generation of interferometers, such as the Square Kilometre Array (SKA)[1], the Murchison Widefield Array (MWA) [3], and the LOw Frequency ARray (LOFAR) [4], surpass conventional sensitivity, resolution, and frequency coverage, correlating unprecedented number of receivers over extremely large areas.

These giant instruments have a hierarchical system architecture in the sense that they are phased-arrays of several smaller phased-arrays (groups of compact receivers) called stations (or subarrays). Consequently, beam-forming techniques adopted within these instruments also follow the same hierarchy, performed initially for individual stations, and later on for the whole instrument.

To exploit full sensitivity potential, station calibration prior to beam-forming is essential. This calibration estimates gain and phase shift compensation parameters, correcting for system losses and delays in station measurements [4, 5, 6, 7]. Most known methods are of the supervised variety, using known properties of known sources to estimate instrumental unknowns. They have two main drawbacks:

- Prior sky information is for strong sources. Disregarding weak sources can considerably affect accuracy [7].
- Performance is sensitive to strong source data accuracy.

Blind, that is unsupervised, calibration works without recourse to previous sky data. As such, it can circumvent the outlined difficulties.

Redundancy calibration [8] is the only blind station calibration method introduced to date. It makes explicit use of redundant baselines, those with the same length and orientation, to repeatedly observe the same resultant Fourier sample of the sky. With sufficient groups of redundant baselines, it can estimate gains and noise more accurately and faster than supervised calibration. Note, however, that such a scheme is only feasible upon deployment of antennas that are entirely devoted to this task, rather than using them for further baselines.

In the context of compressed sensing [9], blind calibration has been introduced as a general sparsity problem which aims to estimate signals along with associated instrumental gain and phase distortions in the absence of additive noise [10]. In this paper, we present a novel application of this approach, using convex optimization for parameter estimation as in [10, 11, 12], to the specific case of radio interferometric station calibration. For this purpose, we extend the blind calibration method to the case of additive noise in measurements. The fundamental reason why it is feasible is that, at low Signal to Noise Ratio (SNR) level in station observations, there are only a few strong sources detectable, with weaker ones buried beneath the noise. Thus, the observations are to all intents and purposes sparse. The proposed blind calibration technique can be applied to any station design and has a very promising performance in the presence of additive noise. It is observable on simulated and real data experiments that the method accomplishes an accuracy superior to the one of supervised calibrations.

The authors acknowledge Ahmad Mouri Sardarabadi, Menno Norden, and ASTRON, for making the LOFAR data available.

[1]http://www.skatelescope.org

1.1. Organisation

Section 2 presents the general measurement model for a station, together with a description of how standard, supervised calibration is performed. In section 3 we propose an extension to blind calibration for compressed sensing [10, 11, 12] which performs in the presence of the additive noise. Furthermore, we examine its computational complexity and suggest ways to reduce it. Using simulations and LOFAR real data, in section 4, we illustrate how considerably higher accuracy than the state of the art – Weighted Alternating Least Squares (WALS) station calibration [5, 7], can be achieved by the proposed blind calibration technique. Finally, we draw our conclusions in section 5.

1.2. Notation

Lowercase bold denotes column vectors (e.g., $\mathbf{g}$), while uppercase bold denotes a matrix (e.g., $\mathbf{R}$). Unless otherwise stated, all values are complex. The Hermitian transpose and the Moore-Penrose pseudo-inverse of a matrix are shown by $(.)^H$ and $(.)^\dagger$, respectively. Frobenius norm is shown by $||.||_F$, and $||.||_1$ denotes the ℓ_1 norm of matrices, which returns the sum of the absolute values of the entries of matrices. Estimated parameters are shown by $\widehat{(\cdot)}$.

2. STATION CALIBRATION

Consider a vector $\mathbf{s} \in \mathbb{C}^Q$ containing signals of Q spatially discrete point sources, approaching a station of P identical receivers placed closely together.

Let $\mathbf{G} = \text{diag}(\mathbf{g})$, where $\mathbf{g} \in \mathbb{C}^P$ denotes the instrumental gain and phase distortions in data, common for all directions in the field of view. Let $\mathbf{B} = \text{diag}(\mathbf{b})$, where $\mathbf{b} \in \mathbb{C}^Q$ represents the receivers' primary (reference) beam [2] in the Q source directions. Finally, let $\mathbf{A} \in \mathbb{C}^{P\times Q}$ be the array response (sensing) matrix expressing the phase shifts in signals associated with the geometry of the receivers and the sources. Then the total signal measured by the receivers in a single time bin, $\mathbf{x} \in \mathbb{C}^P$, can be formulated by [13],

$$\mathbf{x} = \mathbf{GABs} + \mathbf{n},$$

where $\mathbf{n}$ represents the station's additive thermal noise, which is assumed to have i.i.d zero mean complex Gaussian entries.

The receivers of the station collect L measurements $\mathbf{X} = [\mathbf{x}_1, \mathbf{x}_2, \ldots, \mathbf{x}_L] \in \mathbb{C}^{P\times L}$, over a Short Term Integration interval (STI) [13]. Within a STI, the system characteristics, thus $\mathbf{A}$, $\mathbf{B}$, and $\mathbf{G}$, are assumed invariant. Therefore,

$$\mathbf{X} = \mathbf{GABS} + \mathbf{N} \in \mathbb{C}^{P\times L}, \tag{1}$$

where $\mathbf{S} = [\mathbf{s}_1, \mathbf{s}_2, \ldots, \mathbf{s}_L]$, and $\mathbf{N} = [\mathbf{n}_1, \mathbf{n}_2, \ldots, \mathbf{n}_L]$.

[2] Primary beam of a receiver is referred to its direction dependent gain and phase behavior [13]. Identical receivers have identical primary beams.

Standard station calibration is estimation of the direction independent distortions, the P diagonal entries of $\mathbf{G}$, in the measurements, the PL entries of $\mathbf{X}$, using (1). The distortions are introduced by combined effects of system inefficiencies, such as environmental (e.g. temperature) changes, or mismatches in cable lengths of the cables connecting station elements to a common central processing unit. Note that the receivers' primary beam, and therefore $\mathbf{B}$, are mostly known from electromagnetic modeling during the design of the station. However, if this is not the case, station calibration requires to estimate the entries of $\mathbf{B}$ as well [13].

Previous station calibration methods are formulated in terms of the measurements' correlation matrix, estimated by $\widehat{\mathbf{R}} = L^{-1}\mathbf{X}\mathbf{X}^H$. From (1) we get,

$$\mathbf{R} = \mathbf{GAB}\mathbf{\Sigma_s}\mathbf{B}^H\mathbf{A}^H\mathbf{G}^H + \mathbf{\Sigma_n}, \tag{2}$$

where $\mathbf{\Sigma}_s = L^{-1}\mathbf{S}\mathbf{S}^H$ and $\mathbf{\Sigma}_n = L^{-1}\mathbf{N}\mathbf{N}^H$. Since the columns of $\mathbf{S}$ and $\mathbf{N}$ are samples of zero mean white Gaussian random processes, for a large enough sample size L, $\mathbf{\Sigma}_s = \text{diag}([f_1, f_2, \ldots, f_Q])$, and $\mathbf{\Sigma}_n = \text{diag}([\sigma_1^2, \sigma_2^2, \ldots, \sigma_P^2])$, where f_i and σ_j^2 denote the power (flux, variance) of source i, and the noise power (variance) of receiver j, respectively [13]. Therefore, from (2), the general data model of a station is formulated as,

$$\mathbf{R} = \mathbf{GA}\mathbf{\Sigma}\mathbf{A}^H\mathbf{G}^H + \mathbf{\Sigma_n}, \tag{3}$$

where

$$\mathbf{\Sigma} = \mathbf{B}\mathbf{\Sigma_s}\mathbf{B}^H \tag{4}$$

is a diagonal matrix of apparent source powers.

In supervised calibration, the Q sources are assumed to be strong and their positions and intensity known. The exact values of the source power matrix $\mathbf{\Sigma_s}$, and the array response matrix $\mathbf{A}$ then immediately follow. If the receivers' primary beam, $\mathbf{B}$, is known, then from (4), the apparent source powers in $\mathbf{\Sigma}$ are also known. Therefore, supervised station calibration estimates only $\mathbf{G}$ and $\mathbf{\Sigma_n}$ from the data model given by (3). Otherwise, it first estimates $\mathbf{\Sigma}$, and then, using known $\mathbf{\Sigma_s}$ and (4), it estimates the directional gains and phases sampled in $\mathbf{B}$ as well [6, 13, 14]. These estimations can all be obtained with relatively low computational cost [7]. However, weak sources in the field of view, or strong sources located in directions corresponding to low sensitivity of the receiver beams, result in further contributions to the additive noise. This limits calibration accuracy. On top of that, performance is directly linked to the accuracy with which the Q sources, and consequently, $\mathbf{\Sigma_s}$ and $\mathbf{A}$ can be known.

The most commonly used supervised station calibration technique is the Weighted Alternating Least Squares (WALS) station calibration method [5, 7, 14], and as such the main focus of comparison in this paper. It iteratively estimates

$$\{\widehat{\mathbf{G}}, \widehat{\mathbf{\Sigma}}, \widehat{\mathbf{\Sigma}}_\mathbf{n}\} = \underset{\mathbf{G},\mathbf{\Sigma},\mathbf{\Sigma_n}}{\arg\min} \left\| \mathbf{W}(\widehat{\mathbf{R}} - \mathbf{R}(\mathbf{G}, \mathbf{\Sigma}, \mathbf{\Sigma_n}))\mathbf{W} \right\|_F^2,$$

where $\mathbf{W} = \mathbf{R}^{-\frac{1}{2}}$ is the optimal weight matrix.

3. STATION CALIBRATION DONE BLINDLY

We now derive a convex optimization for obtaining instrumental parameters, which does not use a priori information about individual sources in the sky [10, 11]. This calibration can be applied to any station design.

Assume there are $K \gg Q$ directions in the sky from which some signal sources may radiate towards a station. Since the calibration coefficients in $\mathbf{g}$ are non-zero, defining $\mathbf{\Delta} = \mathbf{G}^{-1}$, (1) can be re-parameterized by,

$$\mathbf{\Delta X} = \mathbf{A}(\mathbf{BS} + \mathbf{A}^{\dagger}\mathbf{\Delta N}) = \mathbf{AY}, \tag{5}$$

where

$$\mathbf{Y} = \mathbf{BS} + \mathbf{A}^{\dagger}\mathbf{\Delta N}. \tag{6}$$

If $K > P$, then $\mathbf{A}^{\dagger}$, and consequently, the result of its multiplication to $\mathbf{\Delta N}$, includes $K - P$ dependent rows. Since the row rank of signal matrix $\mathbf{S}$ is roughly Q (there are Q strong sources, plus possibly some weak ignored sources), choosing K so that $K - P \gg Q$ leads to a sparse $\mathbf{Y}$ in (5). Therefore, from $\mathbf{A} \in \mathbb{C}^{P\times K}$ and $\mathbf{X}$ one can estimate

$$\{\widehat{\mathbf{\Delta}}, \widehat{\mathbf{Y}}\} = \arg\min_{\mathbf{Y},\mathbf{\Delta}} \|\mathbf{Y}\|_1 \quad \text{subject to } \mathbf{\Delta X} = \mathbf{AY}, \mathrm{Trace}(\mathbf{\Delta}) = c \tag{7}$$

where $c > 0$ is an arbitrary constant. In this convex optimization, the ℓ_1 norm favors the selection of a sparse $\mathbf{Y}$ among the ones satisfying the problem constraints[3]. The trace constraint ensures the trivial solution $\{\mathbf{0}, \mathbf{0}\}$ is excluded.

The main computation in the optimization (7) is the estimation of the KL entries of $\mathbf{Y}$ (K and L are both larger than P). It can be posed as a Second Order Cone Program (SOCP), and using a primal-dual interior-point method to solve, at most $O\left(\sqrt{2P + 3LK}\right)$ iterations are required, where each iteration has $O\left((2P + 3LK)^2(4 + 4PL + 3KL)\right)$ complexity [15]. This is for a general SOCP. However, the complexity can be reduced due to the sparse structure of the optimization problem (7), and utilizing a smaller number of samples than L for computation.

Note that the convex optimization formulation of blind calibration given by (7) is similar to the one proposed by [10, 11, 12]. But, due to the presence of the additive noise $\mathbf{N}$ in (6), the $\widehat{\mathbf{Y}}$ estimated from (7) is not the true (training) signal which is estimated in the noise-less case studied in [10, 11, 12]. For this particular application of blind calibration to radio interferometric station calibration, however, there is no need to estimate the true signals. The reason is that the output of station calibration which is needed for station beamforming (and later on, for getting correlated with the beamformed signals of the other stations) is in fact $\mathbf{\Delta X}$ [14].

[3] In (7), there are $PL + 1$ equations ($\mathbf{\Delta X} = \mathbf{AY}$, and $\mathrm{Trace}(\mathbf{\Delta}) = c$) constraining $KL + P$ unknowns (entries of $\mathbf{Y}$, and diagonal entries of $\mathbf{\Delta}$). If $PL+1 \geq KL+P$, a unique solution for the blind calibration was simply obtained by solving the equations. Otherwise, the ℓ_1 norm searches for the sparsest solution consistent with the equations.

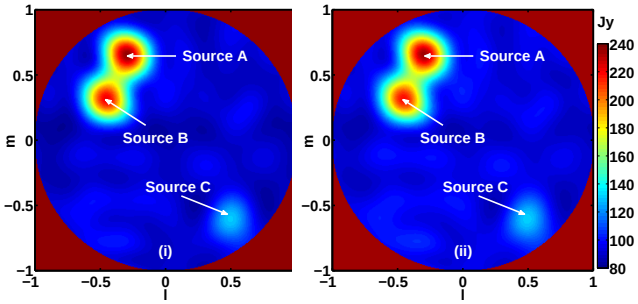

Fig. 1. (i) is the simulated sky image with no calibration, obtained from $\widehat{\mathbf{R}}$. (ii) is the target image with perfect calibration parameters, obtained from $\mathbf{G}^{-1}\widehat{\mathbf{R}}(\mathbf{G}^{-1})^H$.

4. ILLUSTRATIVE EXAMPLES

We now compare the performance of the proposed blind station calibration to that of the WALS method using simulated and real observations.

4.1. Simulation

The configuration details were as follows. A station of $P = 36$ receivers were oriented on a 6×6 nodes rectangular grid. The minimum baseline was 1m. These elements observed a sky consisting of three sources A, B, and C, at (l, m) coordinates $(-0.294, 0.648)$, $(-0.455, 0.322)$, and $(0.486, -0.632)$, and with power equal to $140, 130$, and 40 Jy (Jansky), respectively. The station collected $L = 1200$ samples per STI, at 160 MHz frequency. The elements are assumed to have a uniform primary beam shape ($\mathbf{B} = \mathbf{I}$), and SNR $= 0.1$. The instrumental gains and phases, calibration parameters in $\mathbf{g}$, were drawn from a normal real distribution $\mathcal{N}(1, .2)$ and a uniform real distribution $\mathcal{U}(0, .2)$ respectively. This is considered a realistic simulation of LOFAR [8]. 300×300 pixel images using the beamforming imaging technique [13] were generated.

For comparison purposes, Fig. 1 shows image reconstruction without calibration (from correlation matrix $\widehat{\mathbf{R}} = L^{-1}\mathbf{X}\mathbf{X}^H$) as image (i), and with perfect calibration – using known gains (from corrected correlation matrix obtained by $\mathbf{G}^{-1}\widehat{\mathbf{R}}(\mathbf{G}^{-1})^H$) as image (ii). Note that calibration is executed once per STI, and the resulted parameter estimation, $\widehat{\mathbf{G}}$, is used to correct data from several consecutive STIs. Therefore, image (ii) of Fig. 1 is in fact the target image, in the sense that the same image must be obtained from $\widehat{\mathbf{R}}$ being corrected by calibration solution $\widehat{\mathbf{G}}$. With noise ten times stronger than the signal the blurry images of Fig. 1 look quite similar.

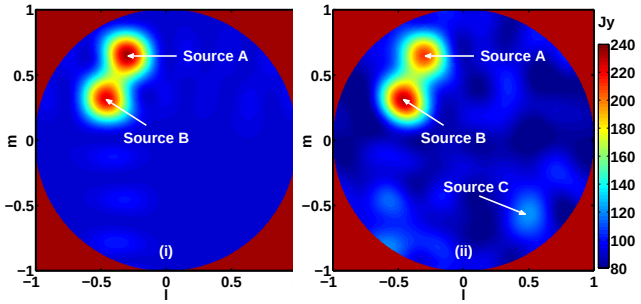

Fig. 2. Images of WALS (i) and blind (ii) calibrations' reconstructed data. WALS underestimates sources A and B, and completely misses source C. Blind calibration accurately reconstructs all three.

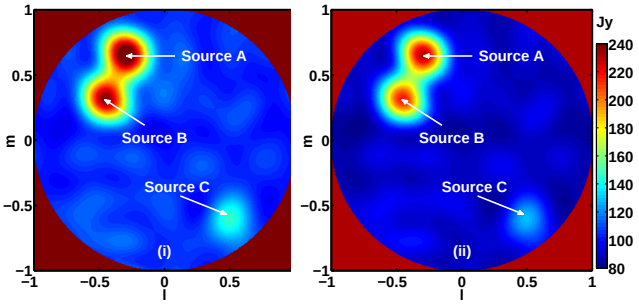

Fig. 3. Images of WALS (i) and blind (ii) calibrations' corrected data. Blind calibration has an image much closer to the target image, image (ii) of Fig. 1.

Calibration method	WALS	Blind
$\|\|\mathbf{g}-\widehat{\mathbf{g}}\|\|_F$	1.3903	0.9925

Table 1. Comparison of the distance between the true parameters $\mathbf{g}$ and the WALS and blind calibrations' estimated parameters $\widehat{\mathbf{g}}$. As the results of the Frobenius norms show, blind calibration solutions are closer to the true parameters.

Now we compare blind and WALS calibration. WALS was most accurate when solving only for the two brightest sources A, B, when their exact powers and coordinates are used. As such, we show this optimistic case. For blind calibration, we made a 9×9 nodes rectangular grid to cover the whole field of view, considering its $K = 81$ nodes as source directions in the sky. The smallest distance between the nodes and any of the three source directions is 12 degrees. Therefore, no node actually matches the positions of the sources. The calibration is run using 250 samples of $\mathbf{X}$.

Consider Fig. 2, which shows images obtained from the data reconstructed by the two calibration techniques. For WALS calibration, the image is obtained from $\mathbf{R}(\widehat{\mathbf{G}}, \widehat{\mathbf{\Sigma}}, \widehat{\mathbf{\Sigma}}_{\mathbf{n}})$, and in the case of blind calibration, it is obtained from $(250)^{-1}\widehat{\mathbf{\Delta}}^{-1}\mathbf{A}\widehat{\mathbf{Y}}\widehat{\mathbf{Y}}^H\mathbf{A}^H\{\widehat{\mathbf{\Delta}}^{-1}\}^H$. WALS calibration underestimates sources A and B by 3 Jy, and completely misses source C. However, blind calibration accurately reconstructs all three. When glancing at the result of blind calibration to image (i) of Fig. 1 this may not be striking. We must, however, take into account that blind calibration used only 250 data samples for estimation. An image constructed from these 250 samples would have no visible difference to the one from blind calibration's reconstructed data.

Fig. 3 shows the images obtained from the corrected data, $\widehat{\mathbf{G}}^{-1}\widehat{\mathbf{R}}(\widehat{\mathbf{G}}^{-1})^H$. We see the superior accuracy achieved by blind calibration, with the image much closer to the target image (image (ii) of Fig. 1) than the one from WALS.

In order to have a quantitative handle on the results, we also calculated the distance between the true (simulated) parameters $\mathbf{g}$ and the WALS and blind calibrations' estimated parameters $\widehat{\mathbf{g}}$. The results are shown in Table 1. Blind calibration achieves a smaller $||\mathbf{g}-\widehat{\mathbf{g}}||_F$, and thus superior accuracy, when compared to WALS calibration.

4.2. Real Observation

We calibrated $L = 1024$ data samples obtained from a single polarization state of $P = 46$ receivers (orthogonal dipoles) of a LOFAR HBA (High Band Antenna) station. The observation is around 3C 401 (Cygnus A, CygA) at 173.2 MHz. Figure 4 demonstrates a 500 pixel image of the data.

We applied WALS and blind calibration to the data. For WALS calibration, the apparent power and position of CygA are used. For blind calibration, similar to section 4.1, a 9×9 nodes rectangular grid is used and calibration is executed only on 250 data samples. Images obtained from the residual of the data subtracted the calibrations reconstructed data are presented in Fig. 5. The residual image of WALS calibration, image (i) of Fig. 5, shows structures observable as the milky way (in red on the left sign). The blind calibration residual, image (ii), is consistant, in contrast, with zero mean random noise. The better performance of blind calibration therefore is clearly shown, which is due to the fact that it considers $K = 81$ potential source directions in the sky, rather than WALS calibration which considers only one (from CygA). The per-

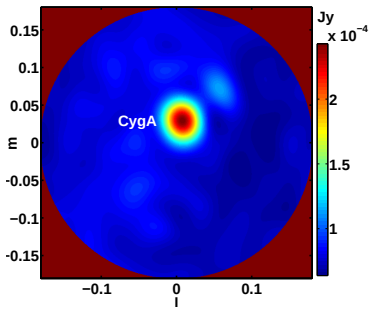

Fig. 4. A CygA observation performed by a single polarization state of receivers of a LOFAR HBA station at 173.2 MHz.

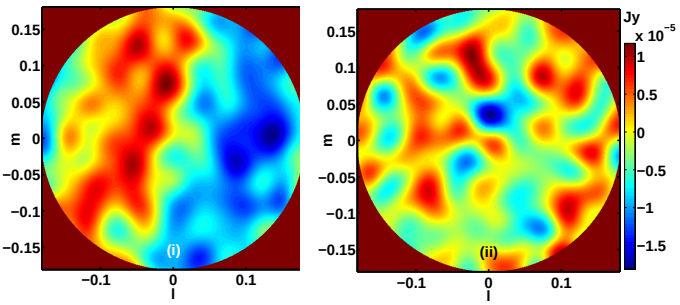

Fig. 5. Residual images around CygA obtained by WALS (i) and blind (ii) calibrations. Clear structures resembling the milky way are observable in (i), while the residual in (ii) resembles that expected from zero mean random noise.

formance of blind calibration gets even more improved by increasing the number of data samples.

5. CONCLUSIONS

The effectiveness of supervised calibration of compact aperture array stations is limited by the SNR of the strongest observed unresolved point sources. Melting low SNR sky objects into background noise limits calibration accuracy. Moreover, performance is based on the accuracy of the properties of the known strongest sources.

We overcome these drawbacks by a novel application of the blind calibration technique using convex optimization [10] to the station calibration problem. It estimates the unknown instrumental parameters based only on a general sparsity assumption on the sky, without using any prior knowledge about its individual sources. Deployable for any station configuration, the proposed blind calibration achieves more accurate solutions than supervised station calibration for the experiments thus far tested.

Its computational complexity is currently higher when compared to alternatives. As such, complexity reduction without loss of accuracy is the main focus of future work. Larger scale testing also merits investigation. This will include Monte Carlo simulations and performance comparison between various convex optimization approaches that can be used for solving the blind calibration problem [12].

6. REFERENCES

[1] A. R. Thompson, J. M. Moran, and G. W. Swenson, Jr., *Interferometry and Synthesis in Radio Astronomy*, John Wiley & Sons, May 2001.

[2] B.F. Burke and F. Graham-Smith, *An Introduction to Radio Astronomy*, Cambridge University Press, 2009.

[3] C. J. Lonsdale and et al., "The Murchison widefield array: Design overview," *Proceedings of the IEEE Special Issue: Advances in Radio Telescopes*, vol. 97, pp. 1497–1506, Aug. 2009.

[4] M. P. van Haarlem and et al., "LOFAR: The LOw-Frequency ARray," *Astronomy & Astrophysics*, vol. 556, pp. A2, Aug. 2013.

[5] A.-J. Boonstra and A.-J. Van Der Veen, "Gain calibration methods for radio telescope arrays," *IEEE Transactions on Signal Processing*, vol. 51, pp. 25–38, Jan. 2003.

[6] A.-J. Boonstra, S. J. Wijnholds, S. van Der Tol, and B. Jeffs, "Calibration, sensitivity and rfi mitigation requirements for lofar," in *IEEE International Conference on Acoustics, Speech, and Signal Processing, (ICASSP 2005)*, Mar. 2005, vol. 5, pp. v/869–v/872 Vol. 5.

[7] S.J. Wijnholds and A.-J. van der Veen, "Multisource self-calibration for sensor arrays," *IEEE Transactions on Signal Processing*, vol. 57, no. 9, pp. 3512–3522, Sept. 2009.

[8] P. Noorishad, *Optimization for high fidelity imaging with aperture array telescopes*, Ph.D. thesis, Kapteyn Astronomical Institute, 2013.

[9] D. L. Donoho, "Compressed sensing," *IEEE Transactions on Information Theory*, vol. 52, no. 4, pp. 1289–1306, Apr. 2006.

[10] R. Gribonval, G. Chardon, and L. Daudet, "Blind calibration for compressed sensing by convex optimization," *ArXiv e-prints*, Nov. 2011.

[11] C. Bilen, G. Puy, R. Gribonval, and L. Daudet, "Blind Sensor Calibration in Sparse Recovery Using Convex Optimization," in *SAMPTA - 10th International Conference on Sampling Theory and Applications - 2013*, Bremen, Germany, Apr. 2013.

[12] C. Bilen, G. Puy, R. Gribonval, and L. Daudet, "Convex optimization approaches for blind sensor calibration using sparsity," *IEEE Transactions on Signal Processing*, vol. 62, no. 18, pp. 4847–4856, Sept. 2014.

[13] Alle-Jan van der Veen and Stefan J. Wijnholds, "Signal processing tools for radio astronomy.," in *Handbook of Signal Processing Systems*, Shuvra S. Bhattacharyya, Ed F. Deprettere, Rainer Leupers, and Jarmo Takala, Eds., pp. 421–463. Springer, 2013.

[14] S.J. Wijnholds, *Fish-eye Observing with Phased Array Radio Telescopes*, 2010.

[15] "Applications of second-order cone programming," *Linear Algebra and its Applications*, vol. 284, no. 13, pp. 193 – 228, Nov. 1998.